Properties of Haldane excitations and multiparticle states in the antiferromagnetic spin-1 chain compound $CsNiCl_3$

M. Kenzelmann,[1] R. A. Cowley,[1] W. J. L. Buyers,[2,3] Z. Tun,[2] R. Coldea,[4,5] and M. Enderle[6,7]
[1]*Oxford Physics, Clarendon Laboratory, Oxford OX1 3PU, United Kingdom*
[2]*Neutron Program for Materials Research, National Research Council of Canada, Chalk River, Ontario, Canada KOJ 1J0*
[3]*Canadian Institute for Advanced Research, Toronto, Ontario, Canada*
[4]*Oak Ridge National Laboratory, Solid State Division, Oak Ridge, Tennessee 37831*
[5]*ISIS Facility, Rutherford Appleton Laboratory, Oxon OX11 0QX, United Kingdom*
[6]*Technische Physik, Gebäude 38, Universität des Saarlandes, 66123 Saarbrücken, Germany*
[7]*Institut Laue-Langevin, BP 156 38042 Grenoble, Cedex 9, France*
(Received 9 December 2001; revised manuscript received 22 March 2002; published 28 June 2002)

We report inelastic time-of-flight and triple-axis neutron scattering measurements of the excitation spectrum of the coupled antiferromagnetic spin-1 Heisenberg chain system $CsNiCl_3$. Measurements over a wide range of wave-vector transfers along the chain confirm that above T_N $CsNiCl_3$ is in a quantum-disordered phase with an energy gap in the excitation spectrum. The spin correlations fall off exponentially with increasing distance with a correlation length $\xi = 4.0(2)$ sites at $T = 6.2$K. This is shorter than the correlation length for an antiferromagnetic spin-1 Heisenberg chain at this temperature, suggesting that the correlations perpendicular to the chain direction and associated with the interchain coupling lower the single-chain correlation length. A multiparticle continuum is observed in the quantum-disordered phase in the region in reciprocal space where antiferromagnetic fluctuations are strongest, extending in energy up to twice the maximum of the dispersion of the well-defined triplet excitations. We show that the continuum satisfies the Hohenberg-Brinkman sum rule. The dependence of the multiparticle continuum on the chain wave vector resembles that of the two-spinon continuum in antiferromagnetic spin-1/2 Heisenberg chains. This suggests the presence of spin-1/2 degrees of freedom in $CsNiCl_3$ for $T \leqslant 12$ K, possibly caused by multiply frustrated interchain interactions.

DOI: 10.1103/PhysRevB.66.024407 PACS number(s): 75.25.+z, 75.10.Jm, 75.40.Gb

I. INTRODUCTION

Nearly two decades after Haldane's conjecture[1] the interest in quantum spin dynamics of low-dimensional antiferromagnets continues unabated. Much of the research is focused on one-dimensional (1D) antiferromagnets with small spin S, where quantum fluctuations are strong because the classical Néel ground state is not an eigenstate of the Hamiltonian. The ground state of such an antiferromagnetic (AF) chain is a spin singlet and long-range magnetic order is absent, even at $T = 0$ K. The spin correlation function in the ground state of AF Heisenberg chains depends on the spin quantum number S: for $S = 1/2$ the spin-spin correlations fall off as a power law with increasing distance (quasi-long-range-ordered ground state) but for $S = 1$ the spin-spin correlations fall off exponentially with increasing distance.[1] The excitation spectrum is also different: for $S = 1/2$ the elementary excitations are spin-1/2 particles called spinons and the spectrum extends to zero energy transfer while for $S = 1$ the elementary excitations are spin-1 particles with a gap (Haldane excitations).

Inelastic neutron scattering is one of the most direct methods to measure the magnetic excitations in solids. In neutron scattering experiments, the spin of the neutron changes by $\Delta S_z = 0, \pm 1$ along a quantization axis so that at low temperatures the response is dominated by broad continua scattering if the elementary particles carry spin 1/2. Sharp modes are observed, however, if the elementary particles carry spin 1. The spectra observed with neutron scattering are therefore fundamentally different in AF spin-1/2 and spin-1 Heisenberg chains: for a spin-1 chain at low temperatures the excitation spectrum is dominated by well-defined modes[2–4] while in the case of a spin-1/2 chain the dominant contribution is a continuum consisting of two-spinon states. The two-spinon continuum has a characteristic wave-vector dependence reflecting the momentum and energy addition of two particles and it has an upper energy boundary at the AF point which is double the maximum single-particle energy and decreases away from it. The observation of such a scattering continuum in a spin system[5] thus clearly suggests that spin-1/2 particles are its elementary excitations rather than spin-1 particles.

Considering the fundamental difference between AF spin-1/2 and spin-1 chains, it came as a surprise when we observed in the spin-1 chain compound $CsNiCl_3$ a multiparticle scattering continuum that resembles the two-spinon continuum of AF spin-1/2 chains.[6] Its wave-vector dependence and its intensity suggest that it does not originate from two- or three-particle excitations of the elementary spin-1 excitations but instead from spin-1/2 degrees of freedom in the system. Their detailed study promises to shed light on the transition from spin-1/2 particles in quantum critical AF spin-1/2 chains and the spin-1 particles found in spin liquids like the gapped Haldane quantum antiferromagnets.

The focus of our previous paper[6] was on the excitation spectrum of the quantum-disordered phase at the AF point $Q_c = 1$ and it was shown with three independent neutron scattering measurements that there is a multiparticle scattering continuum extending from the gapped onset of the exci-

 ©2002 The American Physical Society

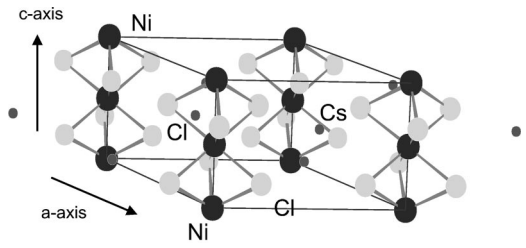

FIG. 1. Crystal structure of $CsNiCl_3$. The Ni atoms are shown as dark spheres, and the Cs and Cl are shown as light spheres. The figure shows four Ni chains on a triangular lattice running along the *c* axis. The Ni atoms are coupled along the *c* axis by an AF superexchange interaction along the Ni-Cl-Ni paths.

tations up to 12 meV. The present paper contains a study of the excitation spectrum for a wide range of wave-vector transfers and for both the well-defined excitations and the multiparticle continuum. For the well-defined excitations the results largely confirm previous results in the quantum-disordered phase of $CsNiCl_3$.[2,7,8] Data measured with a sample mount which consists exclusively of aluminum to avoid any background scattering originating from hydrogenous materials confirm the previous estimate that 12(2)% of the scattering at the AF point $Q_c=1$ is carried by the multiparticle continuum. A detailed description of the multiparticle states is given for a wide range of wave-vector transfers. The integrated intensity of the scattering is shown to be consistent with the first-moment sum rule. The characteristics of the continuum are compared to those of the two-spinon continuum in AF spin-1/2 Heisenberg chains.

II. PROPERTIES OF $CsNiCl_3$

$CsNiCl_3$ is one of the most studied AF coupled spin-1 chain systems. It crystallizes in a hexagonal crystal structure, D_{6h}^4 space group, and the lattice constants at low temperatures are $a=7.14$ Å and $c=5.90$ Å (Fig. 1). The magnetic moments are carried by Ni^{2+} ions which interact via a superexchange interaction involving Cl^- ions. Because the superexchange path along the *c* axis contains only one Cl^- ion and perpendicular to the *c* axis two Cl^- ions (Figs. 1 and 2), the superexchange between the Ni^{2+} ions along the *c* axis is much stronger than perpendicular to the *c* axis. The spin Hamiltonian of $CsNiCl_3$ is that of a system of coupled spin-1 chains with a strong intrachain interaction *J* and a weak interchain interaction J'. It can be written as

$$\mathcal{H}=J\sum_{i}^{\text{chain}}\mathbf{S}_i\cdot\mathbf{S}_{i+1}+J'\sum_{\langle i,j\rangle}^{\text{plane}}\mathbf{S}_i\cdot\mathbf{S}_j-D\sum_i(S_i^z)^2. \quad (1)$$

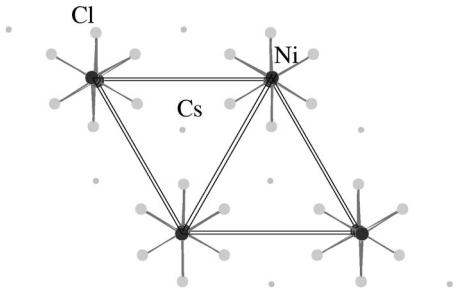

FIG. 2. Crystal structure of $CsNiCl_3$ projected onto the basal plane. The Ni atoms are shown as dark spheres, and the Cs and Cl are shown as light spheres. Ni atoms belonging to different chains are coupled by an AF superexchange interaction along the Ni-Cl-Cl-Ni paths.

The superexchange interaction *J* along the *c* axis was measured with a high-field magnetization measurement of the magnetic saturation field and is 2.28 meV.[9] The superexchange interaction perpendicular to the *c* axis is $J'=0.044$ meV as determined from the measurement of the spin-wave energies in the antiferromagnetically ordered structure at $T=2$ K and comparing them with spin-wave theory.[2,3] The weak easy-axis Ising anisotropy $D=4$ μeV, which was derived from the spin-flop transition field extrapolated to $T=0$ K, is small enough that $CsNiCl_3$ is a good example of an isotropic Heisenberg antiferromagnet.[10]

Due to the interchain interaction, the coupled spin chain system undergoes 3D long-range ordering below $T_N=4.84$ K, where the *c*-axis components of the magnetic moments order.[10] At $T_{\text{canted}}=4.4$ K, the components perpendicular to the *c* axis order too. In the resulting magnetic structure, $\frac{2}{3}$ of the spins are canted away from the *c* axis by 44° at 4.4 K and 59° at 1.6 K,[11,12] due to the easy-axis anisotropy and the magnetic frustration of the triangular lattice. Extrapolated to $T=0$ K, the ordered magnetic moment is $1.05\mu_B$, considerably less than the free-ion value $2\mu_B$.[13] This reduction can be ascribed to strong quantum fluctuations in the 3D ordered phase. Strong quantum fluctuations in the 3D ordered phase are also apparent in the excitation spectrum, where excitations derived from longitudinal Haldane modes were observed which cannot be described by conventional spin-wave theory.[14] Their existence is related to longitudinal fluctuations of the ordered moment, as shown in a calculation of the excitations which includes the gapped Haldane mode coupled to transverse gapless spin-wave-like excitations.[15]

In the quantum-disordered phase above T_N, the excitation spectrum of $CsNiCl_3$ has an energy gap (Haldane gap) (Ref. 2) with a minimum at the AF wave vector. The gap has roughly the energy expected of a Haldane gap, which is a consequence not of a single-ion anisotropy but of strong quantum fluctuations. The excitations are a triplet of well-defined $S=1$ modes,[7,16] and the spin-spin static correlation function falls off exponentially with increasing distance. For wave vectors near the nuclear zone center, a broadening of the excitation spectrum may arise from the theoretically predicted two-particle continuum.[17]

The magnetic susceptibility and the magnetic specific heat have a broad maximum near $T=30$ K,[18,19] which had been traditionally interpreted as the temperature where short-range correlations set in. A neutron scattering experiment showed that the excitations at the AF point persist as a resonance up to at least 70 K,[20,21] so that short-range correlations survive even to temperatures of the order of the spin bandwidth.

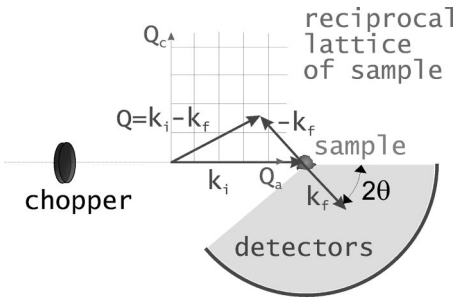

FIG. 3. Schematic drawing of the chopper time-of-flight spectrometer MARI at ISIS. A monochromatic neutron beam is generated using a chopper. The neutrons are scattered at the sample and then detected in the detector banks located at a distance of 4.02 m in a half circle below the sample. Depending on the incident energy and the orientation of the sample, different wave-vector and energy transfer regions are accessed during an experiment.

III. EXPERIMENTAL DETAILS

An inelastic neutron scattering experiment measures the response of a coupled spin system as a function of energy and momentum transfer. The magnetic scattering cross section is directly related to the dynamic structure factors $S^{\alpha\beta}(Q,\omega)$, which are the Fourier transform of the space- and time-dependent spin-pair correlation functions. Defining the neutron energy and momentum transfers to the spin system as $\omega = E_i - E_f$ and $\boldsymbol{Q} = \mathbf{k}_i - \mathbf{k}_f$, respectively, the magnetic scattering cross section for unpolarized neutrons can be written as

$$\frac{d^2\sigma}{d\Omega d\omega} = |f(\boldsymbol{Q})|^2 \frac{k_f}{k_i} \sum_{\alpha,\beta} (\delta_{\alpha\beta} - \hat{Q}_\alpha \hat{Q}_\beta) S^{\alpha\beta}(\boldsymbol{Q},\omega), \quad (2)$$

where $\alpha,\beta = x,y,z$ and $f(\boldsymbol{Q})$ is the magnetic form factor. For a spin system with Heisenberg interactions in the paramagnetic phase, the entire magnetic response is inelastic and the dynamic structure factors have the property $S(Q,\omega) = S^{xx} = S^{yy} = S^{zz}$ because the system has unbroken rotational symmetry. For the Hamiltonian of $CsNiCl_3$, the total z component of spin is a constant of motion if $D\Sigma_i (S_i^z)^2$ is neglected ($S^z = \Sigma_i S_i^z$ commutes with the Hamiltonian) and $S^{\alpha\beta} = 0$ for $\alpha \neq \beta$.

A single crystal of $CsNiCl_3$ $5 \times 5 \times 20$ mm^3 was used for the experiments. The experiments were performed using the triple-axis spectrometer DUALSPEC at the Chalk River Laboratories, Canada and the chopper time-of-flight spectrometer MARI at the pulsed spallation source ISIS of the Rutherford Appleton Laboratory, United Kingdom (see Fig. 3). The sample was kept sealed in an aluminum can containing helium gas to prevent the absorption of water. For the DUALSPEC experiment, the sample was wired to an aluminum plate and placed inside an aluminum can such that no sealant could cause extraneous scattering of neutrons.

The measurements with the DUALSPEC triple-axis spectrometer were performed at 6 K. The sample was mounted in a cryostat with its (hhl) crystallographic plane in the horizontal scattering plane. The scattered neutron energy was set to 14.51 meV. A graphite filter was used to absorb the higher-order reflections from a vertically focusing pyrolytic graphite monochromator and a flat analyzer. The effective collimation from reactor to detector was 39′-48′-51′-72′ and gave an energy resolution of 0.8 meV, as determined from the quasielastic incoherent peak. The longitudinal wave-vector widths of the (002) peak and (220) peak were 0.022 and 0.019 [full width at half maximum (FWHM) in reciprocal lattice units], respectively, and the calculated vertical resolution was 0.29 $Å^{-1}$.

The time-of-flight spectrometer MARI produced a monochromatic beam by means of the Fermi chopper spinning at 150 Hz. The scattered neutrons were detected by an array of He^3 tube detectors typically 30 cm long (perpendicular to the principal scattering plane) and with a diameter of 2.5 cm situated 4.02 m from the sample position. The low-angle bank consists of 136 detectors arranged symmetrically around the incident neutron beam direction and having scattering angles from 3.43 to 13.29°. The detectors in the high-angle banks are arranged in three strips vertically below the sample and cover the scattering angles from 12.43 to 134.14°, where the detector tubes are aligned perpendicular to the vertical scattering plane. The central strip is in the vertical scattering plane, and the two side strips of detectors are out of the vertical plane by an average of 5.56° for high scattering angles. At small scattering angles, the detectors in the two side strips are out of the principal scattering plane by up to 21.36° and the neutrons detected in these detectors have a considerable wave-vector component perpendicular to the scattering plane.

The experiment using MARI was performed with the sample oriented such that the (hhl) crystallographic plane was in the vertical scattering plane and the c axis was perpendicular to the incident beam direction. The incident neutron energy E_i was set either to 20 or 30 meV and the energy resolution was 0.35 and 0.4 meV, respectively, as determined from the FWHM of the quasielastic incoherent scattering peak. The resolution in wave-vector transfer at zero energy transfer was typically 0.02 $Å^{-1}$ along the $c^\star$ axis and along the [110] direction and up to 0.19 $Å^{-1}$ perpendicular to the scattering plane if only the central detector bank was used. Both the energy and the wave-vector resolution improved with increasing energy transfer. The measurements were performed with the sample at temperatures between 6.2 and 12 K. The scattering was measured for a total proton charge between 4000 and 8600 μA h at an average proton current of 170 μA.

The simultaneous measurement of continuous energy transfers ω together with the large range of scattering angles allows the measurement of the dynamical structure factor $S(\mathbf{Q},\omega)$ over the scattering surface, which is a two-dimensional subspace of (Q_a, Q_c, ω), where both Q_a and Q_c lie in the scattering plane. The scattering surface may then be projected down onto the (Q_c,ω) plane and scans with a constant energy transfer or a wave-vector transfer along the chain can be obtained by binning the data appropriately. These scans will henceforth be called constant-ω and constant-Q_c scans, respectively. In our case, because

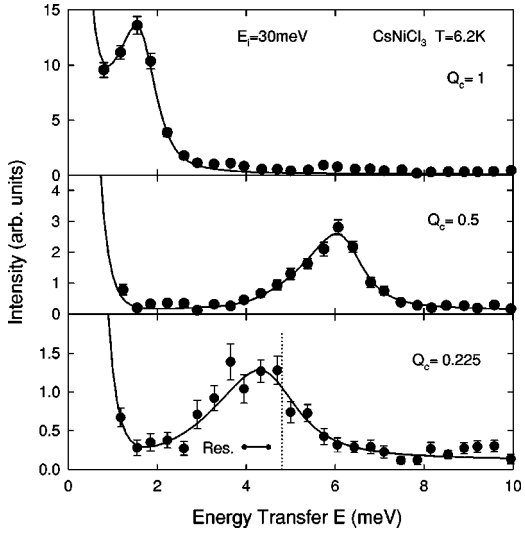

FIG. 4. Neutron scattering intensity at 6.2 K as a function of energy transfer for three different wave-vector transfers Q_c along the chain. The data were measured using the central detector bank of the MARI time-of-flight spectrometer and the wave-vector range sampled for each Q_c in ± 0.025. The incident energy E_i was 30 meV. The tail at lower energies of the well-defined excitations is due to the asymmetric incident beam line shape. The solid line is a fit as described in the text and the dotted line shows the onset of the two-magnon continuum as predicted by the NLσM.

$CsNiCl_3$ is a 1D magnet and the interchain dispersion is sufficiently small, $S(Q_c,\omega)$ mainly reflects the excitation spectrum of the spin chains.

IV. EXPERIMENTAL RESULTS

A. Haldane excitations

The quantum-disordered magnetic phase of $CsNiCl_3$ at temperatures between 6.2 and 12 K was studied for a wide wave-vector and energy range using the MARI time-of-flight spectrometer. Figure 4 shows three constant-Q_c scans at 6.2 K obtained using the binning procedure described above. Only data measured in the central detector bank are shown in Fig. 4. This is because at low scattering angles the two side detector banks are, as mentioned, considerably out of the vertical scattering plane and so the dynamic structure factor $S(\boldsymbol{Q},\omega)$ is different for the three detector banks.

The data are treated as if there was a well-defined excitation and some extra scattering[6] but the data could also be interpreted as a continuum with a well-defined onset at the low-energy boundary. The well-defined excitation has the most intensity at the AF point $Q_c=1$, which corresponds to a π phase difference between the Ni spins along the chains. The intensity decreases towards $Q_c=0.5$, but it is visible down to $Q_c=0.2$. The scattering was fitted with an antisymmetrized Lorentzian form weighted by the Bose factor

$$S(\boldsymbol{Q},\omega)=A[n(\omega)+1]\times\left(\frac{\Gamma}{[\omega-\epsilon(\boldsymbol{Q})]^2+\Gamma^2}-\frac{\Gamma}{[\omega+\epsilon(\boldsymbol{Q})]^2+\Gamma^2}\right) \quad (3)$$

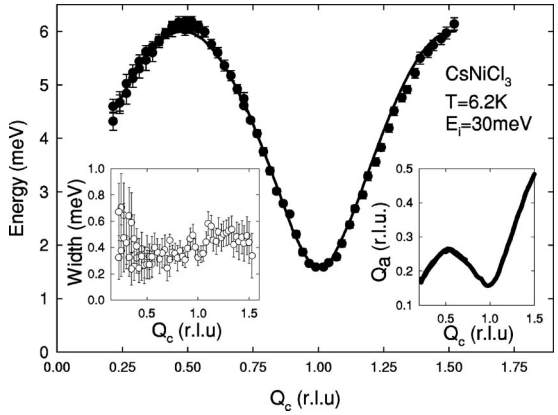

FIG. 5. Excitation energy as a function of wave-vector transfer Q_c along the chain. The solid line is a fit to the excitation energy as described in the text. Left inset: Lorentzian half width Γ as a function of wave-vector transfer Q_c along the chain. Right inset: wave-vector transfer along $[Q_a,Q_a,0]$ and Q_c calculated from the fitted energy transfer and Q_c.

and convoluted with the line shape of the quasielastic incoherent scattering, which is a good estimate of the resolution particularly at low-energy transfers. Here, $\epsilon(\boldsymbol{Q})$ is the dispersion relation, Γ is the excitation width, $n(\omega)+1$ is the population factor, ω is the neutron energy transfer, and A is a scaling constant. For the excitations close to $Q_c=1$, we found that a Lorentzian line shape gave fits with consistently lower sum of discrepancies χ^2 than for an antisymmetrized Gaussian cross section, in agreement with our measurements obtained using the RITA spectrometer.[20,21] The fits give a good description of the magnetic excitation spectra including the tail at lower energies of the well-defined excitations which is due to the asymmetric incident beam line shape (Fig. 4 and 6).

Fits were performed to obtain the intensity, the frequency, and the width of the well-defined excitations. An energy-independent background increasing with the wave-vector transfer Q_c along the chain was chosen such that the scattering at high-energy transfers matches the scattering at low energies below the well-defined excitation. The excitation energy and width are shown in Fig. 5. The data for $Q_c>1.6$ were not analyzed due to their contamination with phonons. The maximum of the dispersion is 6.19(9) meV, in agreement with previous measurements,[3] and the excitation energy at $Q_c=1$ is 1.59(5) meV.

The observed dispersion of a single AF spin-1 chain is often written phenomenologically as[4]

$$\omega(Q_c)=\sqrt{\Delta^2+v_s^2\sin^2(Q_c\pi)+\alpha^2\cos^2\left(\frac{Q_c}{2}\pi\right)}, \quad (4)$$

where Δ is the Haldane gap, v_s is the spin velocity, and α determines the asymmetry of the dispersion about $Q_c=0.5$. For a two-particle gap of 2Δ as $Q_c\to 0$ one would expect $\alpha=\sqrt{3}\Delta$. Because the chains are coupled in $CsNiCl_3$, the excitations have a dispersion perpendicular to the chain direction. The coupling of the chains can be taken into account

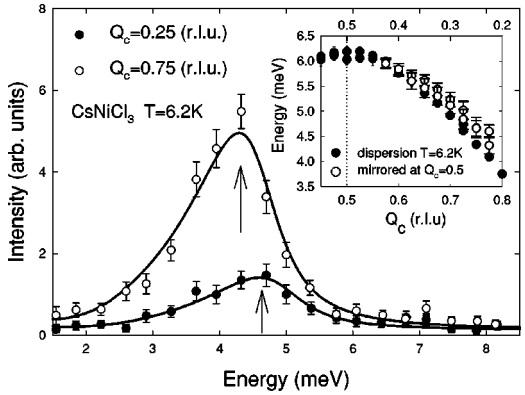

FIG. 6. Neutron scattering intensity as a function of energy transfer for $Q_c=0.25$ and $Q_c=0.75$. The energy of the excitation at $Q_c=0.25$ is clearly higher than at $Q_c=0.75$. Inset: The solid circles represent the excitation energy for $Q_c>0.5$ (bottom axis) and the open circles data for $Q_c<0.5$ (top axis), both corrected for the Q_a dependence of the dispersion. Hence the dispersion is not periodic about $Q_c=0.5$. The tail at lower energies of the well-defined excitations is due to the asymmetric incident beam line shape.

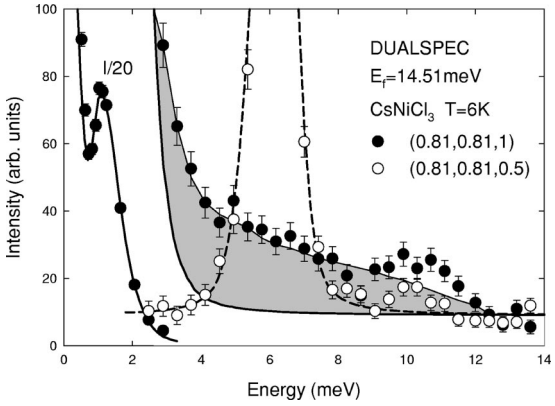

FIG. 7. Neutron scattering intensity at $\boldsymbol{Q}=(0.81,0.81,1)$ (solid circles) as a function of energy transfer measured using the DUALSPEC triple-axis spectrometer. The scattering intensity below 3 meV is shown 20 times reduced. The scattering at $\boldsymbol{Q}=(0.81,0.81,0.5)$ is shown for comparison (open circles). The solid and dashed line are fits to the measured spectra as explained in the text.

in a random phase approximation (RPA) and the dispersion relation can be written as[22]

$$\omega^2(\boldsymbol{Q})=\omega(Q_c)[\omega(Q_c)+2J'(Q_a,Q_b)\cdot S(\boldsymbol{Q})]. \qquad (5)$$

$S(\boldsymbol{Q})$ is the static structure factor and $J'(Q_a,Q_b)$ is the Fourier transform of the exchange interaction perpendicular to the chain axis. The Fourier transform $J'(Q_a,Q_a)$ along the reciprocal $[1,1,0]$ direction, which is of relevance for the present experiment, is given by

$$J'(Q_a,Q_a)=J'[4\cos(2\pi Q_a)+2\cos(4\pi Q_a)], \qquad (6)$$

and vanishes for $Q_a=0.19$. The static structure factor falls rapidly as $|Q_c-1|$ increases, weakening the effect of the interchain exchange interaction on the dispersion.

The solid line in Fig. 5 corresponds to a fit of Eq. (5) to the observed dispersion during which J' was kept fixed so that $\omega(\frac{2}{3},\frac{2}{3},1)=0.4$ meV.[7] The fitted parameters are $\Delta=1.24(4)$ meV$=0.54(2)J$, $v_s=5.70(7)$ meV$=2.50(3)J$, and $\alpha=2.5(3)$ meV$=1.1(1)J=2.0\Delta$.

Δ is consistent with our previous measurements[20] and is higher than the gap energy of 1.14 meV calculated for the nonlinear σ model[23] (NLσM) which includes the temperature renormalization at 6.2 K. This is possibly due to an additional upward renormalization of the gap energy caused by the coupling of the spin chains.[20] The observed energy at $Q_c=1$, $\omega=1.59(5)$ meV, is higher than Δ because it corresponds to an excitation with a different wave-vector transfer perpendicular to the chain axis. For weakly coupled spin chains Δ can be directly measured at $\boldsymbol{Q}=(0.19,0.19,1)$ where the Fourier transform of the interchain coupling vanishes. In this experiment, however, the gap excitation could only be sampled at $\boldsymbol{Q}=(0.16,0.16,1)$ as shown in the right inset of Fig. 5, and here the excitation energy is higher.

The spin velocity v_s is in excellent agreement with numerical results predicting $v_s=2.5J$.[24,25] α is consistent with previous results obtained for NENP (Ref. 4) and $CsNiCl_3$ (Ref. 26) and its nonzero value reflects the asymmetry of the dispersion with respect to reflection at $Q_c=0.5$ as would occur for a simple antiferromagnet. Figure 6 shows the asymmetry about $Q_c=0.5$ as measured using the MARI spectrometer. The figure compares two equivalent scans at $Q_c=0.25$ and $Q_c=0.75$, and the excitation at $Q_c=0.75$ clearly has a lower energy than the one at $Q_c=0.25$. Due to the dependence of the excitations on Q_a (right inset of Fig. 5), the energy difference between the two observed excitations is increased compared with what would have been observed for an isolated spin-1 chain. We applied the correction for this Q_a dependence of the dispersion by using Eq. (5) and the Q_a dependence of the excitations (inset of Fig. 5) to extract the dispersion of an uncoupled chain. The 3D corrected dispersion is shown in the inset of Fig. 6 showing that the energy of the excitation towards $Q_c=0$ is clearly higher than towards $Q_c=1$.

The Q_c dependence of the excitation width (Fig. 5) suggests a crossover from a one-particle dispersion for $Q_c>0.5$ to a two-particle continuum with a corresponding increased excitation width for $Q_c<0.5$. The crossover from a one-particle to a two-particle response has also been observed by Zaliznyak *et al.*[26] at 1.5 K in the 3D ordered phase. In their experiment the increase in width is clearer because the thermal broadening of the one-particle peaks is much less. In both experiments the broadened peaks are centered at energies lower than the onset of the two-particle continuum for noninteracting chains (Fig. 5). Possibly this is because of the 3D interchain coupling which at 1.5 and 6.2 K gives considerable dispersion to the excitation energies for $Q_c=1$ as Q_a varies. This could decrease the two-particle onset energy.

B. Continuum scattering

Figure 7 shows two constant-$\boldsymbol{Q}$ scans measured using the DUALSPEC triple-axis spectrometer at the Chalk River

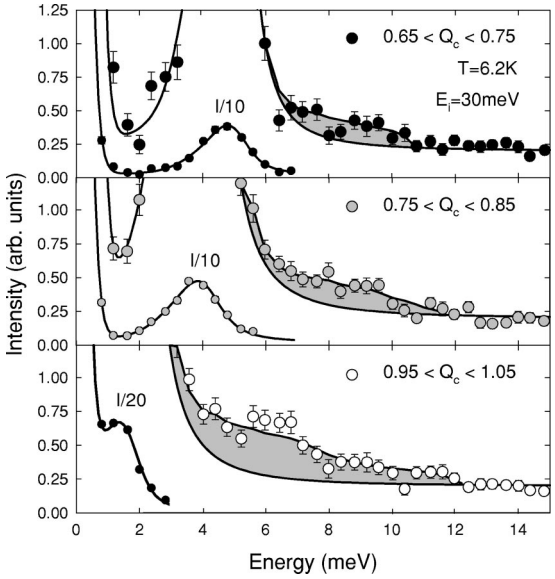

FIG. 8. Neutron scattering spectrum at 6.2 K for various wave-vector transfers. The peak intensities are scaled to fit onto the graph. The lower solid lines are fits to the peak data and the upper line is a guide to the eye enclosing the shaded area of the continuum scattering. The data were obtained on the MARI spectrometer with $E_i = 30$ meV.

Laboratories and compares the scattering at the AF point $\boldsymbol{Q} = (0.81,0.81,1)$ with that at $\boldsymbol{Q} = (0.81,0.81,0.5)$, both at $T = 6$ K. For $Q_c = 1$ new data with the sample mounted so that no hydrogenous material was in the beam are presented. The data are corrected for neutron absorption. This was done by measuring the quasielastic scattering when the sample presented the same angles to the incident and scattered beams as in the constant-$\boldsymbol{Q}$ scans. At $Q_c = 0.5$, where the dispersion of the well-defined excitation has a maximum, the scattering intensity below and above the sharp excitation is considerably lower than the intensity at $Q_c = 1$, and it gives a good measure of the nonmagnetic background. The excess scattering at $Q_c = 1$ at energies above the single-particle excitation is the continuum scattering.

The well-defined excitation at $\boldsymbol{Q} = (0.81,0.81,1)$ is well described by an antisymmetrized Lorentzian weighted by the Bose factor and convoluted with the resolution ellipsoid given by Cooper and Nathans,[27] but it does not account for the continuum scattering. After subtracting phonon scattering near 10 meV, which was estimated from measurements at large wave vectors, the integrated continuum intensity is 9(2)% of the total intensity at $\boldsymbol{Q} = (0.81,0.81,1)$, consistent with the previous estimate of 12(2)%.[6]

The wave-vector dependence of the multiparticle continuum on Q_c was measured at 6.2 K using the time-of-flight spectrometer MARI. Three constant-Q_c scans at $\langle Q_c \rangle = 0.7$, $\langle Q_c \rangle = 0.8$, and $\langle Q_c \rangle = 1$ shown in Fig. 8 confirm that for energies higher than the energy of the well-defined excitation, a slowly decreasing intensity is observed for all three wave-vector transfers.

The observed spectra were fitted by an antisymmetrized Voigt function weighted by the Bose factor and convoluted with the line shape of the quasielastic incoherent scattering peak, which should give a good account of the energy resolution at low-energy transfers. A Voigt function, which is a convolution of a Lorentzian with a Gaussian function, is needed to account for the extra energy width resulting from the wide wave-vector resolution $\Delta Q_c = 0.1$. The fits give a good account of the well-defined excitations (Fig. 8), but do not account for the scattering at higher energies associated with the multiparticle continuum. For $\langle Q_c \rangle = 1$, the scattering extends up to about 12 meV. The scattering at $\langle Q_c \rangle = 0.8$ and $\langle Q_c \rangle = 0.7$ extends to slightly lower-energy transfers, indicating a decreasing upper energy boundary of the continuum with increasing $|Q_c - 1|$.

In order to confirm that the extra scattering is not a resolution artifact, a series of tests using a spectrometer simulation program available at ISIS were made to investigate whether the continuum above the well-defined excitations could result from the convolution of the neutron resolution function with the single-mode dispersion. The program takes into account the spectrometer parameters—the detailed pulse line shape, the chopper characteristics, the position and dimensions of the detectors, etc.—and predicts the scattering line shape for a particular sample orientation and model cross section. The results of this simulation reproduced the measured line shape of the quasielastic incoherent scattering and of the well-defined excitations, and showed that none of the scattering at higher energies could arise from the tail of the resolution function.

We also investigated whether the scattering continuum can be influenced by neutron scattering by phonons. Measurements were performed at 8, 12, and 200 K, with an incident energy of $E_i = 20$ meV and with the 1D axis oriented perpendicular to the incident neutron beam direction. The scattering intensity, normalized to the incident beam monitor, is shown in Fig. 9 at different temperatures.

Above 5 meV, the intensity of the continuum scattering does not change between 6 and 12 K (Fig. 13). We then averaged the spectra at 8 and 12 K to obtain better statistics at high energy transfers for $\langle T \rangle = 10$ K. This leads to an artificial broadening of the well-defined excitations, and so the averaged data at low-energy transfers were not analyzed in detail.

The upper panel in Fig. 9 compares the neutron scattering intensity at $Q_c = 1$ measured with MARI in the quantum disordered phase at $\langle T \rangle = 10$ K (8–12 K) with that measured at 200 K. The lower panel of Fig. 9 shows the imaginary part of the generalized susceptibility $\chi''(Q_c = 1,\omega) = S(Q_c = 1,\omega)/[n(\omega)+1]$ obtained from the dynamic structure factor. Yet at 200 K, $\chi''(Q_c = 1,\omega)$ is clearly less than at $\langle T \rangle = 10$ K for all energy transfers, apart from a sharp peak at 11.5 meV which can be associated with a single-phonon excitation. It is not present in the measurements with incident energy $E_i = 30$ meV which sampled a different scattering surface. If the continuum scattering between 5 and 12 meV for $\langle T \rangle = 10$ K were due to neutron scattering by phonons, $\chi''(\pi,\omega)$ would be comparable at 200 K. The fact that it decreases greatly shows that the slowly decreasing scattering intensity above the Haldane mode is magnetic and not phonon scattering. At $T = 200$ K, $\chi''(Q_c = 1,\omega)$ has a broad peak at ~ 5 meV, as we will discuss in a forthcoming publication.[21] This broad peak is absent at low temperatures

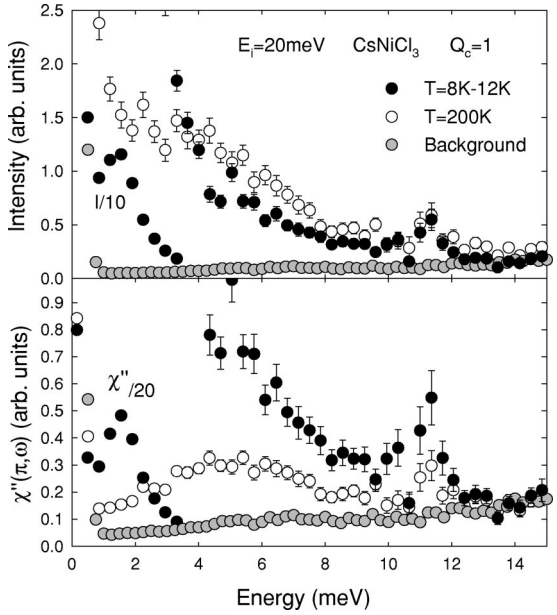

FIG. 9. Upper panel: neutron scattering spectrum at $Q_c=1$, at the average of $T=8$ and 12 K (solid circles) and at $T=200$ K (open circles). The intensity was integrated for $0.9<Q_c<1.1$. The data were measured using the MARI spectrometer and $E_i=20$ meV. Lower panel: the imaginary part of the magnetic susceptibility $\chi''(\pi,\omega)$ as a function of energy transfer for the quantum-disordered phase at low temperatures and in the high-temperature limit. The gray solid circles show the background estimated from the scattering detected at high scattering angles as described in the text.

when only low-energy magnetic excitations are thermally activated and $\chi''(\pi,\omega)$ is dominated by the slightly-broadened Haldane gap mode.

An estimate of the nonmagnetic background was also obtained from the scattering observed in detectors at high scattering angles 2Θ for which the wave-vector transfer $|\mathbf{Q}|$ is large, and the magnetic form factor is low so that the spectrum is dominated by the phonon scattering which is proportional to $|\mathbf{Q}|^2$ or $|\mathbf{Q}|^4$.[28] The nonmagnetic background for the low-angle scans was estimated by scaling the high-angle intensity as $|\mathbf{Q}|^2$. The background that is independent of $|\mathbf{Q}|$ was estimated from the energy gain side of the spectrum at low temperatures. The estimate for the background including coherent and incoherent multi-phonon scattering is shown in Fig. 9 as gray solid circles. This estimate does not include scattering from well-defined single phonon excitations. Assuming that the whole intensity at high scattering angles scales with $|\mathbf{Q}|^2$ or that part of the scattering scales with $|\mathbf{Q}|^4$ leads to a yet smaller background. The estimated nonmagnetic background scattering accounts only for a small fraction of the observed scattering at $Q_c=1$ up to 12 meV and substantiates the magnetic origin of the observed continuum.

The momentum dependence of the continuum shows a broad maximum at $Q_c=1$. Figure 10 compares two constant-ω scans for $\langle\omega\rangle=10$ meV and for $\langle\omega\rangle=14$ meV; the latter can be taken as the background. The constant-ω data were obtained by integrating the intensity between 8 and 12 meV and between 12 and 16 meV, respectively. Thus the magnetic scattering from the well-defined excitation was not included in the integration, while the results for $\langle\omega\rangle=14$ meV are a measure of the background.

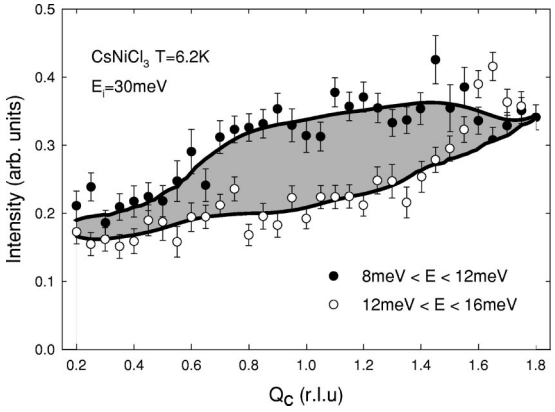

FIG. 10. Neutron scattering intensity at $T=6.2$ K as a function of wave-vector transfer along the chain, Q_c, and integrated between 8 and 12 meV (solid circles) and integrated between 12 and 16 meV (open circles). Lines are guides to the eye. The data were measured in all three detector banks of the MARI spectrometer with an incident energy $E_i=30$ meV.

Figure 10 shows that for wave-vector transfers $0.6<Q_c<1.4$, the scattering intensity for $\langle\omega\rangle=10$ meV is higher than for $\langle\omega\rangle=14$ meV. The fact that the additional scattering is located around the AF zone center is further evidence for its magnetic origin.

The energy-integrated intensity of the multiparticle states for $0.5<Q_c<1$ is shown in Fig. 11 as a fraction of the total scattering intensity at $Q_c=1$ at the 1D point (0.81,0.81,1). It was determined numerically from the measured intensity after the integrated intensity of the well-defined excitation was subtracted. Figure 11 shows that the energy-integrated intensity of the continuum has its maximum at $Q_c=1$ and approaches zero for $Q_c=0.5$. The integrated intensity is smaller near $Q_c=0.5$ partly because the range of energies for which the multiparticle continuum can be observed gets smaller as the momentum decreases.

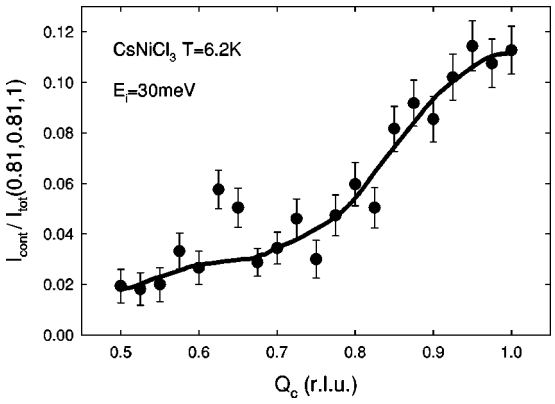

FIG. 11. Energy-integrated continuum scattering at $T=6.2$ K as a fraction of the integrated intensity at (0.81,0.81,1) and as a function of wave-vector transfer Q_c along the chain. The data is corrected for the magnetic form factor. The solid line is a guide to the eye.

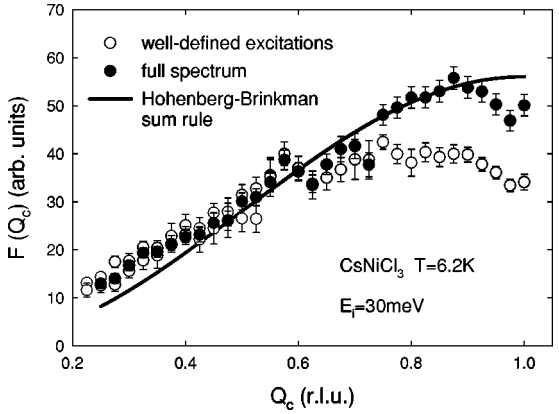

FIG. 12. $F(Q_c)=\int d\omega\, \omega\, S(Q_c,\omega)$ at $T=6.2$ K as a function of the wave-vector transfer Q_c along the chain. Solid circles show $F(Q_c)$ calculated numerically from the observed spectra; open circles represent $F(Q_c)$ of the well-defined excitations. The solid line is the result of the Hohenberg-Brinkman sum rule.

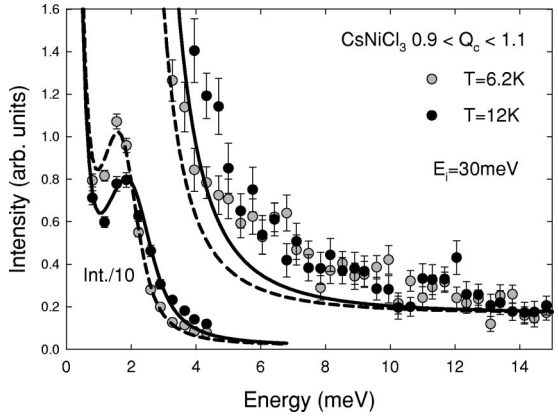

FIG. 13. Neutron scattering intensity as a function of energy transfer for wave-vector transfer with $0.9<Q_c<1.1$ at 6.2 and 12 K. The peak from the Haldane gap mode is shown with its intensity reduced by a factor of 10. The lines are fits of a Lorentzian function to the observed intensity at 6 K (dashed line) and 12 K (solid line).

Sum rule. A further test of the magnetic nature of the continuum scattering is provided by the Hohenberg-Brinkman first-moment sum rule. The first energy moment $F(Q_c)=\int d\omega\, \omega\, S(Q_c,\omega)$ of 1D magnets with nearest-neighbor exchange interaction is given by $F(Q_c)\propto[1-\cos(\pi Q_c)]$.[29] This relation is valid even in the presence of a weak interchain coupling constant.[30] The first energy moment $F(Q_c)$ was determined from the observed spectra after subtracting a flat background and correcting for the magnetic form factor. The contribution from the well-defined excitation is shown in Fig. 12 as open circles and from the total scattering by the solid circles. The solid line is the prediction of the Hohenberg-Brinkman sum rule which predicts that the first moment doubles between $Q_c=0.5$ and $Q_c=1$. It is clear that the observed spectrum is consistent with the sum rule, while $F(Q_c)$ determined from the well-defined excitations alone is not. This result confirms that the multiparticle continuum is magnetic, that the single-mode approximation fails, and that the presence of the continuum is required to fulfill the sum rule.

The presence of the high-energy continuum has important consequences for the static structure factor $S(Q_c)$. Because scattering at higher energies enters the first moment with a higher weight than low-energy scattering, $S(Q_c)$ is smaller if high-energy excitations are present. Since the continuum is most intense for $Q_c=1$ and lower for increasing $|Q_c-1|$, the width of $S(Q_c)$ as a function of Q_c is expected to increase around $Q_c=1$, corresponding to a reduced correlation length. This is what we have indeed observed (see later).

Temperature dependence. The temperature dependence of the multiparticle continuum was investigated between 6.2 and 12 K. Figure 13 compares the scattering intensity at $Q_c=1$ for 6.2 and 12 K. The two spectra were measured in the same configuration, with the incident energy $E_i=30$ meV and the c axis perpendicular to the incident neutron beam direction. At the higher temperature, the well-defined excitation has a higher energy and becomes wider, consistent with our previous triple-axis measurements.[20] The model of the antisymmetrized Lorentzian function weighted by the Bose factor describes the well-defined excitations well, but the fits cannot account for the scattering at higher energies (Fig. 13). At both $T=6.2$ and 12 K the multiparticle scattering extends up to about 12 meV. Between 6.2 and 12 K the multiparticle scattering is largely independent of temperature and the scattered intensity between 5 and 12 meV energy transfer is the same at both temperatures. This result was used earlier[6] to average the two data sets to produce a color plot with increased statistics.

The upward renormalization of the excitation energy and the broadening of the excitation with increasing temperature increases the scattering at higher energy transfers as the temperature is increased. Much above 12 K the multiparticle states cannot be distinguished unambiguously from the broadened single particle excitation.[20,21]

C. Correlation length

The instantaneous structure factor at $T=6.2$ K for the 1D chain, $S(Q_c)$, is shown in Fig. 14. It was determined experimentally by integrating the scattering observed with the MARI spectrometer over both the well-defined excitations and the continuum scattering. The background scattering was subtracted, the remaining scattering corrected for the magnetic form factor dependence and then integrated numerically up to energy transfers of 12 meV to give $S(\boldsymbol{Q})$. In the experiment the intensity was measured close to but not exactly at the noninteracting wave vector (inset in Fig. 5). The structure factor of the independent chain was obtained from $S(\boldsymbol{Q})$ by assuming as for antiferromagnets that the integrated intensity of the excitations close to the AF point is proportional to $1/\omega(\boldsymbol{Q})$ and the 1D structure factor is given by

$$S(Q_c)=\frac{\omega(\boldsymbol{Q})}{\omega(Q_c)}S(\boldsymbol{Q}), \tag{7}$$

where $\omega(Q_c)$ and $\omega(\boldsymbol{Q})$ are given by Eqs. (4) and (5).

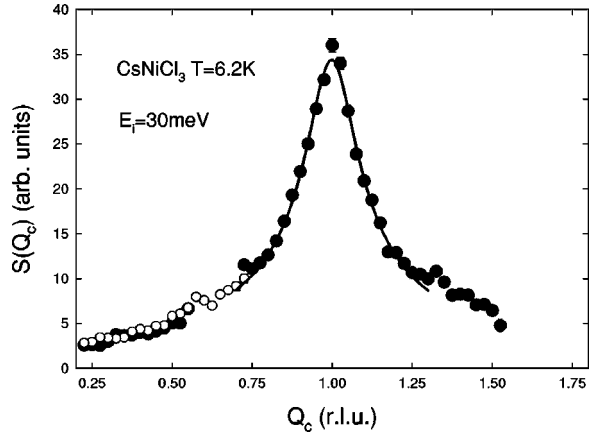

FIG. 14. Static from factor $S(Q_c)$, for the wave-vector transfer Q_c along the chain as a function of energy transfer at $T=6.2$ K. The open circles represent data measured at negative wave-vector transfer Q_c and reflected at $Q_c=0$. The solid line is a fit to the data, based on Eq. (12), as explained in the text.

If the correlations along the chains decay exponentially, as for a 1D Ising model, the structure factor is given by

$$S_I(Q_c)=S^2\frac{\sinh(\xi_I^{-1})}{\cosh(\xi_I^{-1})+\cos(\pi Q_c)}, \tag{8}$$

where the correlation length ξ_I is measured in spin steps $c/2$ along the chain. If $\xi \gg 1$ and $|Q_c-1| \ll 1$, then this can be approximately written as a Lorentzian

$$S_I(Q_c)=\frac{2\xi_I}{1+\pi^2(Q_c-1)^2\xi_I^2}. \tag{9}$$

When this function is convoluted with a Gaussian to take account of the wave-vector range sampled along the chain direction and fitted to the $S(Q_c)$ shown in Fig. 14, the correlation length obtained is 2.2(2) spins. It would be only 1.9(1) spins if the 3D correction, Eq. (7), is neglected because the data near $Q_c=1$ were taken for $Q_a<0.19$ where $S(\boldsymbol{Q})$ is suppressed.

The theory of the structure factor of $S=1$ linear chains is usually formulated using the single-mode approximation in which it is assumed that all the spectral weight resides in a mode whose energy coincides with the first moment $\omega(Q_c)$ of the Hohenberg-Brinkman sum rule:[29]

$$S^{\alpha\alpha}_{\mathrm{SM}}(Q_c)=-\frac{4}{3}\frac{\langle\mathcal{H}\rangle}{L}\frac{(1-\cos\pi Q_c)}{\hbar\omega^{\alpha\alpha}(Q_c)}, \tag{10}$$

where $\langle\mathcal{H}\rangle/L$ is the ground-state energy per spin. Using Eq. (4) for $\omega(Q_c)$, $S(Q_c)$ near $Q_c=1$ is proportional to a square-root Lorentzian

$$S_{\mathrm{SM}}(Q_c)\propto\frac{\xi}{\sqrt{1+\pi^2(Q_c-1)^2\cdot\xi^2}}, \tag{11}$$

where we expect

$$\xi=\frac{\sqrt{v_s^2+\alpha^2/4}}{\Delta}. \tag{12}$$

In Eq. (11) we neglect a small logarithmic term necessary to conserve the total spin. When our experimental values of v_s, α and Δ are inserted we expect $\xi=4.8(2)$.

The square-root Lorentzian gives a better description of the data in Fig. 14 than the Lorentzian, Eq. (9). After convoluting Eq. (11) with a Gaussian to take account of the wave-vector range sampled for each Q_c and fitting to the data between $0.7<Q_c<1.3$, we find $\xi=4.0(2)$ sites and if the 3D correction, Eq. (7), is neglected 3.0(2) sites. The value of 4.0(2) is less than $\xi=5$ from numerical calculations for isolated chains.[31] It is also less than the value of 4.8(2) deduced from the parameters of the well-defined excitations, indicating that the single-mode approximation is not entirely valid. The correlation length deduced from Eq. (11) is shorter because of the presence of the continuum, which depresses $S(Q_c)$ near $Q_c=1$ as may be seen from the first-moment sum rule. Qualitatively the continuum excitations at high energy contribute less to $S(Q_c)$ than would a spectrum that was entirely confined to low-energy excitations.

The observed value of ξ at 6.2 K is much lower than the result reported by Zaliznyak *et al.*[8] This is because their measurements were performed with wave vectors close to the minimum of the excitation energy at $\boldsymbol{Q}_{\mathrm{order}}=(0.33,0.33,1)$. Consequently, the results are strongly influenced by 3D effects because the correlation length measured at this wave vector diverges at the 3D ordering temperature T_N. Those results cannot therefore be compared with the correlation length of isolated quantum chains. Furthermore, Zaliznyak *et al.*[8] performed the energy integration only up to energy transfers of 1.6 meV and our results show that there is appreciable scattering at higher-energy transfers. This effect and their chosen wave-vector transfer both give rise to a larger correlation length that that observed in our experiment.

V. DISCUSSION

With improved measurements of the gapped quantum-disordered spin system $CsNiCl_3$ at 6.2 K we have mapped out the behavior of weakly coupled spin-1 chains. We find (1) that the Haldane excitations have a spin velocity $v_s=5.70(7)$ meV$=2.5$ J—in excellent agreement with field theory[32] and numerical calculations[25,31,33,34]—(2) that the single-chain correlation length is shorter than that of isolated chains, and (3) that the observed multiparticle continuum at the AF point carries about 12(2)% of the total scattering. This confirms previous experimental results[6] that the continuum is much larger than expected theoretically.

A. Continuum

Multi-particle continua for AF wave vectors have been predicted for $T=0$ K in the framework of the NLσM and numerical techniques. In the framework of the NLσM the continuum consists of three-particle states whose dynamic structure factor has a energy gap of $3\Delta_0$ and a pronounced

maximum in its intensity at $\sim 6\Delta_0$ (Δ_0 is the Haldane gap energy at zero temperature).[35,36] Its continuum integrated intensity from $3\Delta_0$ up to $20\Delta_0$ is only a tiny fraction, 1%, of the total scattering at $Q_c=1$, even if the coupling of the magnetic chains are taken into account in a RPA.[36]

The diagonalization of the quantum eigenstates of a spin-1 chain with $N=20$ sites predicts that at $Q_c=1$ the Haldane excitation carries 97% of the total scattering,[37] leaving no more than 3% of the scattering weight to contribute to continuum scattering. More precise results can be obtained using the density matrix renormalization group method. These calculations show that at $T=0$ K the Haldane excitation in a spin-1 chain with $N=256$ sites carries 97.6(1)% of the total scattering at $Q_c=1$,[38] predicting thus at least 2.4 times more scattering than the NLσM. This discrepancy is not very surprising because the three-particle states at higher energies involve excitations far away from the AF wave vector where the field theory is known not to give accurate results.

Clearly none of the theories can explain our observed result of 12% continuum scattering. We conclude therefore that the multiparticle continuum observed in $CsNiCl_3$ is not in accordance with theoretical results for an isolated AF spin-1 Heisenberg chain with nearest-neighbor interactions at $T=0$ K.

B. Comparison to Majorana fermion theory

Other models for AF spin-1 chains assume that the spins also interact via biquadratic exchanges. Biquadratic spin interactions are thought to be small in most materials, but they cannot be ruled out *a priori*. The Hamiltonian for these models can be written as

$$\mathcal{H}=J\sum_{i}^{\text{chain}} \mathbf{S}_i\cdot\mathbf{S}_{i+1}+b(\mathbf{S}_i\cdot\mathbf{S}_{i+1})^2. \tag{13}$$

This Hamiltonian can be exactly solved for $b=-1$ (Armenian point) and for $b=1/3$ which is the valence-bond solid (VBS). It has been shown numerically that the energy gap of this Hamiltonian is nonzero for $-1<b<1$ with a maximum at $b=0.41$.[39] Close to the Armenian point, the spin system can be treated in the framework of Tsvelik's Majorana fermion theory,[40] which is a low-energy field theory for linear spin-1 chains. This theory predicts that the multiparticle scattering states carry 17% of the intensity at $Q_c=1$ for b close to -1.[36]

A strong biquadratic term ($b=1$) not only increases the spectral weight of the multi-particle continuum it also reduces the energy gap[39] in the excitation spectrum to zero. This is not in accordance with the facts. In $CsNiCl_3$ the single-chain gap Δ at 6.2 K is higher than expected from the bilinear exchange J. This suggests that biquadratic interactions are weak and that the observed magnetic multiparticle continuum cannot be explained by the Majorana fermion theory.

C. Correlation length

The single-chain correlation length ξ has been determined to be $\xi=4.0(2)$, which is considerably shorter than $\xi=5$ obtained from quantum Monte Carlo calculations for finite chains at $T=0.25J\simeq 6.2$ K.[31] Since the measurements of ξ were made close to the noninteracting wave vector, $Q_a=0.81$, they should give the correlation length of isolated chains. Nevertheless, the discrepancy may arise if the RPA approximation, Eq. (5), does not remove all of the 3D effects adequately.

The ground state of an isolated chain has a hidden string order. It is composed of states such as $|+-+-0+00-0+\rangle$ in which the antiferromagnetic ordering is maintained across intervening zero ($S_z=0$) sites. Possibly this order is destroyed more effectively by 3D interactions than is predicted by the RPA.

The strong quantum fluctuations in $S=1$ linear chains are largely due to the low spin and low dimensionality. The fluctuations may further be enhanced, and the correlation length decreased, if there are frustrated interactions. In $CsNiCl_3$ there are two possibilities for frustrated interactions. First, the chains are arranged on a hexagonal lattice, so there are bound to be frustrated interactions between the chains arranged at the corners of the triangle. A second possibility is that the interchain interactions may be between not only spins in the same basal plane but also between spins in the neighboring chains that are at $\pm c/2$ along the chains.[41] If these interactions are also strong and antiferromagnetic, as might be the case for superexchange interactions, then even the interactions between pairs of chains are at least partially frustrated.

Further theoretical work is needed to understand whether these multiply frustrated interchain interactions are responsible for the shortened correlation length as well as the associated upward renormalization of the Haldane gap[20] or whether the effects result from a failure of the RPA.

D. Origin of the continuum

We first compare with a material with smaller 3D interactions. $Ni(C_2H_8N_2)_2NO_2ClO_4$ (NENP) is a AF spin-1 chain system in which the interchain couplings are not frustrated and much smaller than in $CsNiCl_3$, but a large single-site anisotropy splits the three Haldane excitations into two distinct excitations.[42] For NENP at 0.3 K the ratio of the first moment at the AF point and at the maximum of the dispersion is $R=F(1)/F(0.5)\sim 1.8(3)$ for the weighted average of the doublet and singlet excitations if data published by Ma *et al.*[4] are used for the calculations, and this is in agreement with the theoretical value 2.[29] Neglecting the multiparticle continuum in $CsNiCl_3$ this same calculation yields $R=1.2(2)$. This shows that in contrast to $CsNiCl_3$, the sharp excitations in NENP are enough to fulfill the Hohenberg-Brinkman sum rule and no magnetic weight is expected at higher energy transfers as in $CsNiCl_3$ at 6.2 K. Any continuum would be hard to observe even in highly deuterated NENP because of residual hydrogen scattering. Because NENP has weaker 3D interactions, this comparison suggests

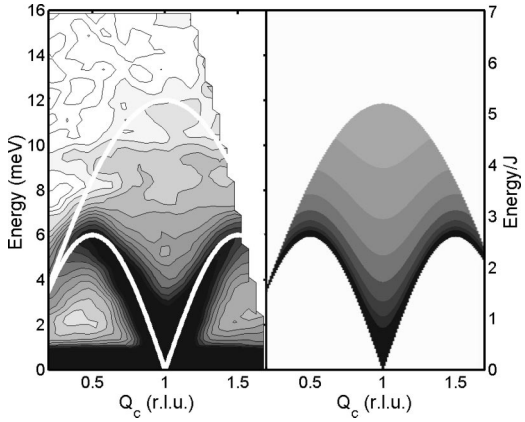

FIG. 15. Left panel: scattering intensity observed in $CsNiCl_3$ at $T=6.2$ K as a function of wave-vector transfer Q_c and energy transfer on a logarithmic scale. The data were measured with an incident energy $E_i=30$ meV. Data measured in detectors at high scattering angles are not shown. Right panel: scattering intensity expected for a spin-1/2 chain according to the Müller ansatz as a function of wave-vector transfer and energy transfer (in units of J) (Ref. 43). The energy axis of the Müller ansatz was scaled so that the lower bound of the two-spinon continuum matches the maximum of the single-particle dispersion in $CsNiCl_3$.

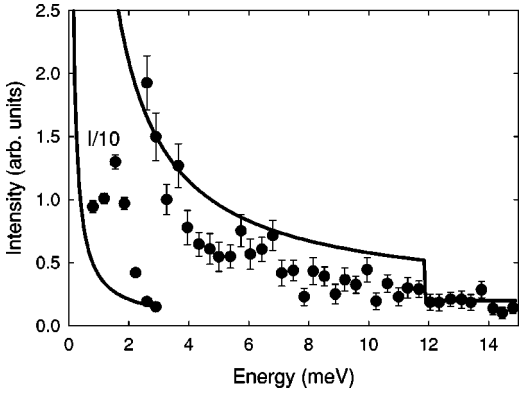

FIG. 16. Measured scattering intensity of $CsNiCl_3$ at $\langle Q_c\rangle=1$ and at $T=6.2$ K as a function of energy transfer. The solid line is the scattering intensity expected from a spin-1/2 chain according to the Müller ansatz.

that interchain interactions may be responsible for generating the continuum observed in $CsNiCl_3$.

We speculate that the multiparticle continuum is generated by the AF coupling of the spin-1 chains and multiply frustrated interchain interactions might be decisive for the size of the effect. A shortened AF correlation length—due to a frustration-induced enhancement of quantum fluctuations—has two main effects on the dynamic structure factor at $Q_c=1$. First, it leads to an additional upward renormalization of the gap energy which is proportional to $1/\xi$ [see Eq. (12)]. Second, a decreased correlation length results in a reduced structure factor $S(Q_c=1)$ because the total scattering must be constant [Eq. (11)]. Additionally there is strong evidence that the absolute value of $S(\mathbf{Q}=(0.81,0.81,1))$ at low temperatures is smaller than that of isolated chains by at least 1.6.[30] If only a well-defined mode existed, it would have to increase its energy at $Q_c=1$ by a factor of 1.6 to satisfy the first-moment sum rule of Hohenberg and Brinkman.[29] However, the Haldane energy is only 20% higher relative to an uncoupled chain and so the increase of Haldane energy is insufficient to compensate for the loss of intensity. The *only* way for the system to comply with the sum rule is to create a scattering continuum at high energies, as we find it does. This is evidence that the observed continuum in $CsNiCl_3$ is correlated with an enhancement of quantum fluctuations due to multiply frustrated 3D spin correlations.

E. Similarity to the two-spinon continuum of spin-1/2 chains

Figure 15 compares the observed intensity at 6.2 K (left panel) with the scattering expected for an AF spin-1/2 chain based on the Müller ansatz[43] (right panel). The peak of the lower energy boundary of the two-spinon continuum was chosen to match the maximum of the single-particle dispersion in $CsNiCl_3$ for direct comparison of the two excitation spectra. The experimentally observed integrated intensity $I_{\rm tot}=\int dQ_c\int d\omega\, S(Q_c,\omega)$ of $CsNiCl_3$ with $S=1$ was set equal to $S(S+1)=2$. The intensity of the Müller ansatz, which is valid for chains with $S=1/2$, was scaled to $2S(S+1)=1.5$ (the factor of 2 accounts for the spin-1/2 components per Ni^{2+} site arising from the two holes in the d shell of the Ni^{2+} ion).

The two excitation spectra in Fig. 15 have obvious similarities: the multiparticle continuum extends to approximately 12 meV, which is twice the maximum of the one-particle energy, and the upper boundary of the continuum decreases with increasing distance from the AF point. Both continuum spectra can be described with a lower boundary $\omega_{\rm min}=\omega_{\rm AFZB}|\sin(Q_c\pi)|$ (the experiment could not establish whether the continuum scattering is gapped or not) and an upper boundary $2\omega_{\rm max}=\omega_{\rm AFZB}\sin(Q_c\pi/2)$, where $\omega_{\rm AFZB}=6$ meV. Qualitatively the continuum spectrum found in $CsNiCl_3$ has similar features to the continuum found in AF $S=1/2$ chains.[5]

The intensity of the continuum in a spin-1/2 chain is much stronger than that in $CsNiCl_3$. This is shown in Fig. 16, which compares the scattering at $Q_c=1$ as a function of energy transfer for $CsNiCl_3$ and for a spin-1/2 chain. The lines of equal intensity are also different in the two cases (Fig. 15). At 7 meV, as an example, the intensity in $CsNiCl_3$ is constant, while it has a clear minimum at $Q_c=1$ for the Müller ansatz.

We conclude that the intensity and the wave-vector dependence of the observed continuum suggests that a small amount of spin-1/2 degrees of freedom are generated in $CsNiCl_3$, possibly by multiply frustrated interchain interactions. In analogy to the excitations in a spin-1/2 chain, the excitations in $CsNiCl_3$ may therefore also be described by a single spectral function containing a sharp onset and a continuum at higher energies. We found that the spectral functions given by field theory[44] are indeed able to describe both the well-defined excitation and the multiparticle continuum close to the AF point if the critical exponents are adjusted, suggesting that the well-defined excitation is an onset of a

scattering continuum. More theoretical work is needed to clarify the spectral function and its dependence on the 3D interactions as the likely source of the multiparticle states.

VI. CONCLUSIONS

In summary, the excitation spectrum of $CsNiCl_3$ has been measured between 6.2 and 12 K. The results confirm that the spin system is in a quantum-disordered phase and the excitation spectrum has its full $Q_c=2$ periodicity. The single-chain correlation length at 6.2 K is 4.0(2) sites along the chain, which is lower than the value predicted by quantum Monte Carlo calculations, possibly due to spin correlations perpendicular to the chain axis. The reduced correlation length and the associated upward renormalization of the Haldane gap underlines the need for more powerful theoretical tools to describe the frustrated AF coupling of quantum chains.

The key result is the observation of a magnetic multiparticle continuum for wave vectors $0.6<Q_c<1.4$ along the chain. The magnetic multiparticle states have higher energies than the well-defined excitations and extend up to about twice the maximum in the one-particle dispersion. The integrated intensity of the multiparticle continuum is much larger than that predicted for the three-particle continuum by field theoretical models and numerical techniques for AF spin-1 chains with nearest-neighbor exchange interaction. The observed multiparticle continuum resembles the two-spinon continuum of AF spin-1/2 chains, but its intensity is weaker. This suggests the presence of spin-1/2 degrees of freedom in the quantum-disordered phase just above the ordering temperature, possibly generated by competing interactions due to the 3D AF interactions.

ACKNOWLEDGMENTS

We would like to thank O. Petrenko (ISIS), S. M. Bennington (ISIS), and R. L. Donaberger (Chalk River) for their assistance with experiments and A. Zheludev (Oak Ridge National Laboratory), P. Santini (Oxford University), F. H. L. Essler (Warwick University), and I. Affleck (University of British Columbia) for enlightening discussions. Financial support for the experiments was provided by the EPSRC, by the EU through its Large Installations Program and by the British Council-National Research Council Canada Program. ORNL is managed for the U.S. DOE by UT-Battelle, LLC, under Contract No. DE-AC05-00OR22725. One of the authors (M.K.) was supported by the Swiss National Science Foundation under Contract No. 83EU-053223.

[1] F. D. M. Haldane, Phys. Rev. Lett. **50**, 1153 (1983).
[2] W. J. L. Buyers, R. M. Morra, R. L. Armstrong, M. J. Hogan, P. Gerlach, and K. Hirakawa, Phys. Rev. Lett. **56**, 371 (1986).
[3] R. M. Morra, W. J. L. Buyers, R. L. Armstrong, and K. Hirakawa, Phys. Rev. B **38**, 543 (1988).
[4] S. Ma, C. Broholm, D. H. Reich, B. J. Sternlieb, and R. W. Erwin, Phys. Rev. Lett. **69**, 3571 (1992).
[5] D. A. Tennant, T. G. Perring, R. A. Cowley, and S. E. Nagler, Phys. Rev. Lett. **70**, 4003 (1993).
[6] M. Kenzelmann, R. A. Cowley, W. J. L. Buyers, R. Coldea, J. S. Gardner, M. Enderle, D. F. McMorrow, and S. M. Bennington, Phys. Rev. Lett. **87**, 017201 (2001).
[7] M. Steiner, K. Kakurai, J. K. Kjems, D. Petitgrand, and R. Pynn, J. Appl. Phys. **61**, 3953 (1987).
[8] I. A. Zaliznyak, L.-P. Regnault, and D. Petitgrand, Phys. Rev. B **50**, 15 824 (1994).
[9] A. A. Katori, Y. Ajiro, T. Asano, and T. Goto, J. Phys. Soc. Jpn. **64**, 3038 (1995).
[10] H. Kadowaki, K. Ubukoshi, and K. Hirakawa, J. Phys. Soc. Jpn. **56**, 751 (1987).
[11] D. E. Cox and V. J. Minkiewicz, Phys. Rev. B **4**, 2209 (1971).
[12] W. B. Yelon and D. E. Cox, Phys. Rev. B **7**, 2024 (1973).
[13] V. J. Minkiewicz, D. E. Cox, and G. Shirane, Solid State Commun. **8**, 1001 (1970).
[14] M. Enderle, Z. Tun, W. J. L. Buyers, and M. Steiner, Phys. Rev. B **59**, 4235 (1999).
[15] I. Affleck and G. F. Wellman, Phys. Rev. B **46**, 8934 (1992).
[16] Z. Tun, W. J. L. Buyers, R. L. Armstrong, E. D. Hallman, and D. P. Arovas, J. Phys. (Paris), Colloq. **49**, C1-1431 (1988).
[17] I. Affleck and R. A. Weston, Phys. Rev. B **45**, 4667 (1992).
[18] N. Achiwa, J. Phys. Soc. Jpn. **27**, 561 (1969).
[19] D. Moses, H. Shechter, E. Ehrenfreund, and J. Makovsky, J. Phys. C **10**, 433 (1977).
[20] M. Kenzelmann, R. A. Cowley, W. J. L. Buyers, and D. F. McMorrow, Phys. Rev. B **63**, 134417 (2001).
[21] M. Kenzelmann, R. A. Cowley, W. J. L. Buyers, R. Coldea, M. Enderle, and D. F. McMorrow (unpublished).
[22] Z. Tun, W. J. L. Buyers, R. L. Armstrong, K. Hirakawa, and B. Briat, Phys. Rev. B **42**, 4677 (1990).
[23] T. Jolicoeur and O. Golinelli, Phys. Rev. B **50**, 9265 (1994).
[24] E. S. Sorensen and I. Affleck, Phys. Rev. B **49**, 13 235 (1994).
[25] E. S. Sorensen and I. Affleck, Phys. Rev. B **49**, 15 771 (1994).
[26] I. A. Zaliznyak, S.-H. Lee, and S. V. Petrov, Phys. Rev. Lett. **87**, 017202 (2001).
[27] M. J. Cooper and R. Nathans, Acta Crystallogr. **23**, 357 (1967).
[28] G. L. Squires, *Thermal Neutron Scattering* (Cambridge University Press, Cambridge, England, 1978).
[29] P. C. Hohenberg and W. F. Brinkman, Phys. Rev. B **10**, 128 (1974).
[30] M. Kenzelmann and P. Santini (unpublished).
[31] Y. J. Kim, M. Greven, U. J. Wiese, and R. J. Birgeneau, Eur. Phys. J. B **4**, 291 (1998).
[32] D. V. Kveshchenko and A. V. Chubukov, Sov. Phys. JETP **66**, 1088 (1987).
[33] M. Takahashi, Phys. Rev. Lett. **62**, 2313 (1989).
[34] E. S. Sorensen and I. Affleck, Phys. Rev. Lett. **71**, 1633 (1993).
[35] M. D. P. Horton and I. Affleck, Phys. Rev. B **60**, 11 891 (1999).
[36] F. H. L. Essler, Phys. Rev. B **62**, 3264 (2000).
[37] M. Takahashi, Phys. Rev. B **50**, 3045 (1994).
[38] T. D. Kühner and S. R. White, Phys. Rev. B **60**, 335 (1999).

[39] U. Schollwöck, T. Jolicoeur, and T. Garel, Phys. Rev. B **53**, 3304 (1996).
[40] A. M. Tsvelik, Phys. Rev. B **42**, 10 499 (1990).
[41] T. Kambe, H. Tanaka, S. Kimura, H. Ohta, M. Motokawa, and K. Nagata, J. Phys. Soc. Jpn. **65**, 1799 (1996).
[42] J. P. Renard, L. P. Regnault, and M. Verdaguer, J. Phys. (Paris) **49**, 1425 (1988).
[43] G. Müller, H. Thomas, H. Beck, and J. C. Bonner, Phys. Rev. B **24**, 1429 (1981).
[44] H. J. Schulz, Phys. Rev. B **34**, 6372 (1986).